AMERICAN SOCIETY FOR MICROBIOLOGY | mSystems

Check for updates

| Open Peer Review | Environmental Microbiology | Research Article

Single-colony MALDI mass spectrometry imaging reveals spatial differences in metabolite abundance between natural and cultured *Trichodesmium* morphotypes

Karl J. Romanowicz,[1] Futing Zhang,[2,3] Siyuan Wang,[2,3] Dušan Veličković,[4] Rosalie K. Chu,[4] Yeala Shaked,[2,3] Rene M. Boiteau[1,5]

AUTHOR AFFILIATIONS See affiliation list on p. 14.

ABSTRACT *Trichodesmium*, a globally significant N_2-fixing marine cyanobacterium, forms extensive surface blooms in nutrient-poor ocean regions. These blooms consist of a dynamic assemblage of *Trichodesmium* species that form distinct colony morphotypes and are inhabited by diverse microorganisms. *Trichodesmium* colony morphotypes vary in ecological niche, nutrient uptake, and organic molecule release, differentially impacting ocean carbon and nitrogen biogeochemical cycles. Here, we assessed the poorly studied spatial abundance of metabolites within and between three morphologically distinct *Trichodesmium* colonies collected from the Red Sea. We also compared these results with two morphotypes of the cultivable *Trichodesmium* strain IMS101. Using matrix-assisted laser desorption/ionization (MALDI) mass spectrometry imaging (MSI) coupled with liquid extraction surface analysis (LESA) tandem mass spectrometry (MS^2), we identified and localized a wide range of small metabolites associated with single-colony *Trichodesmium* morphotypes. Our untargeted MALDI-MSI approach revealed 80 unique features (metabolites) shared between *Trichodesmium* morphotypes. Discrimination analysis showed spatial variations in 57 shared metabolites, accounting for 62% of the observed variation between morphotypes. The greatest variations in metabolite abundance were observed between the cultured morphotypes compared to the natural colony morphotypes, suggesting substantial differences in metabolite production between the cultivable strain IMS101 and the naturally occurring colony morphotypes that the cultivable strain is meant to represent. This study highlights the variations in metabolite abundance between natural and cultured *Trichodesmium* morphotypes and provides valuable insights into metabolites common to morphologically distinct *Trichodesmium* colonies, offering a foundation for future targeted metabolomic investigations.

IMPORTANCE This work demonstrates that the application of spatial mass spectrometry imaging at single-colony resolution can successfully resolve metabolite differences between natural and cultured *Trichodesmium* morphotypes, shedding light on their distinct biochemical profiles. Understanding the morphological differences between *Trichodesmium* colonies is crucial because they impact nutrient uptake, organic molecule production, and carbon and nitrogen export, and subsequently influence ocean biogeochemical cycles. As such, our study serves as an important initial assessment of metabolite differences between distinct *Trichodesmium* colony types, identifying features that can serve as ideal candidates for future targeted metabolomic studies.

KEYWORDS matrix-assisted laser desorption/ionization (MALDI), liquid extraction surface analysis (LESA), mass spectrometry imaging (MSI), untargeted metabolomics, *Trichodesmium*, colony morphotypes, metabolite abundance

Editor Laura-Isobel McCall, San Diego State University, San Diego, California, USA

Address correspondence to Rene M. Boiteau, rboiteau@umn.edu.

Karl J. Romanowicz and Futing Zhang contributed equally to this article. Author order was determined both alphabetically and in order of seniority.

The authors declare no conflict of interest.

See the funding table on p. 15.

Received 26 August 2024
Accepted 9 September 2024
Published 24 September 2024

Trichodesmium spp. are a globally important bloom-forming diazotrophic cyanobacteria prevalent throughout oligotrophic tropical and subtropical ocean regions (1). Responsible for up to 50% of marine N_2-fixation (2, 3), *Trichodesmium* is considered a vital player in the biogeochemical carbon and nitrogen cycles of the global ocean. A distinctive characteristic of *Trichodesmium* is its ability to exist either as individual filaments (trichomes) (4) or as millimeter-sized colonies composed of tens to hundreds of individual trichomes (5). *Trichodesmium* colonies form an array of different morphotypes, generally classified as spherical shapes termed "puffs" or fusiform shapes termed "tufts" (4). This colonial lifestyle has been proposed as a key to *Trichodesmium's* ecological success and biogeochemical role as a nitrogen "fertilizer" of ocean productivity (6). Colony formation is advantageous for diversifying metabolic activity, elevated mobility in the water column, and acquisition of scarce nutrients from aerosols and particles (6–8). Metabolic rates such as N_2-fixation, denitrification, and nutrient uptake were reported to vary among *Trichodesmium* colony morphotypes, along with differences in buoyancy and chemical gradients of dissolved oxygen and pH (9, 10). However, the underlying metabolic differences related to the observed differences in morphotype behavior are not well understood, largely due to the challenges in analyzing metabolites in these naturally occurring colonies.

Trichodesmium is a highly versatile organism, with colony formation characteristics that vary among its species and across different ocean basins (4). Studies on both natural populations and laboratory isolates have uncovered complex and sometimes contradictory traits, including the genetic identity of colonies, the plasticity of morphotype shapes, and the timing and triggers for colony formation [e.g., references (6, 8, 11)]. For example, the lab-cultivated strain IMS101, composed exclusively of *Trichodesmium erythraeum (T. erythraeum*), typically grows as free trichomes (12–14). However, it can also form colonies during the late stationary growth phase when nutrients are depleted, biomass is high, and pH increases (8, 15), or when exposed to high levels of turbulence (16), or high irradiance and oxidative stress (12). These cultured morphotypes often serve as proxies for natural colony morphotypes that cannot currently be maintained in long-term laboratory cultures. In nature, *Trichodesmium* colonies can consist of one or multiple *Trichodesmium* species, and the colony phenotype, referred to here as a morphotype, is not necessarily linked to a specific genotype (14, 17). For example, in the Northern Red Sea, the site studied here, puff-shaped morphotypes are predominantly associated with *Trichodesmium thiebautii* (*T. thiebautii*), while tuft-shaped morphotypes are primarily dominated by *T. erythraeum* (17). However, the puff-shaped colonies that appear as two distinct puff morphotypes, dense and thin, are both dominated by a single *T. thiebautii* genotype (17). Despite these recognized differences in taxonomy and physiological state between morphotypes, little is known about metabolic differences between them.

Natural *Trichodesmium* colonies also exhibit a more diverse array of functional characteristics than cultivated strains [e.g. references (16, 18)]. For instance, thin puffs bind to and center dust more rapidly than dense puffs, suggesting the regulation of distinct metabolisms (19). Additionally, *Trichodesmium* colonies host a diverse assemblage of other microorganisms (i.e., epibionts), including bacteria, eukaryotic phytoplankton, protists, and zooplankton, often referred to as a joint microbiome (11, 20, 21). Associated bacteria from Red Sea *Trichodesmium* colonies harbor functional traits, including quorum sensing and siderophore biosynthesis, which likely contribute to overall colony function and resource acquisition (22). However, assessing the metabolic differences that relate to colony morphotypes has remained a challenge, largely due to the sporadic occurrence and, at times, low biomass of these colonies, which preclude obtaining sufficient material for conventional metabolomic analyses.

To investigate the metabolic similarities and differences between distinct *Trichodesmium* morphotypes, sensitive metabolomic comparison of a small number of colonies is needed. One promising approach is matrix-assisted laser desorption/ionization mass spectrometry imaging (MALDI-MSI) analysis of single colonies. MALDI-MSI is a powerful tool for spatially resolved metabolomics analysis in complex biological systems (23, 24). MALDI-MSI can detect a broad range of metabolites with very low sample volume requirements (capable of several micron lateral resolution) and tolerance for salty samples, making it particularly suitable for mapping metabolites across the surface of a single *Trichodesmium* colony. The use of a high-resolution Fourier transform-ion cyclotron resonance mass spectrometer (FT-ICR MS) for MALDI-MSI further enables assignments of a detected metabolite's molecular formula (25, 26). A limitation of MALDI-FT-ICR MSI is the inability to resolve mass isomers due to a lack of sensitivity and throughput for tandem mass spectrometry (MS^2) measurements, as it is based only on MS^1 analysis where mass isomers have the same exact mass. Recently, it has been demonstrated that liquid extraction surface analysis (LESA) coupled with Orbitrap mass spectrometry can provide complementary structural information on metabolites from a sample by decoupling the desorption and ionization steps, which enables sensitive MS^2 fragmentation spectra and subsequent fragmentation analysis for a broad range of metabolites within a single probing area (24, 27).

Here, we employed MALDI-MSI combined with LESA-MS^2 fragmentation spectra to analyze the metabolomes of single *Trichodesmium* colonies and draw comparisons between different natural and cultured morphotypes to distinguish metabolites that discriminate them. Our study focused on natural colonies isolated from the Red Sea and morphotypes of the laboratory-grown *Trichodesmium* strain IMS101. Our goals were to (i) develop the application of MALDI-MSI at single-colony resolution to resolve metabolite differences between natural and cultured *Trichodesmium* morphotypes, (ii) evaluate the pairing of MALDI-MSI results with LESA-MS^2 fragmentation analysis to confidently annotate a broad range of metabolites associated with single-colony *Trichodesmium* morphotypes, and (iii) investigate the spatial distribution of discriminant metabolites across natural and cultured *Trichodesmium* colonies to aid in future targeted metabolomics studies. The results of this study demonstrate major differences between *Trichodesmium* morphotypes that provide targets for future studies that elucidate their role in colony formation.

MATERIALS AND METHODS

Natural and cultured *Trichodesmium* morphology collection

To assess the spatial differences in metabolite abundance between natural and cultured colony morphologies of *Trichodesmium*, natural colony morphotypes were sampled from Red Sea bloom-forming *Trichodesmium* populations and compared with the cultivable *Trichodesmium* strain IMS101 grown as single trichomes or as a colony-forming morphotype (Fig. 1). Natural colonies of *Trichodesmium* were sampled throughout the spring bloom (April to June 2021) using a 100-µm phytoplankton net at 10–20 m depth in the Gulf of Aqaba (Eilat, Israel; 29.56°N, 34.95°E). Three distinct morphotypes (tuft shaped, thin puff shaped, and dense puff shaped) were then handpicked using a plastic dropping pipette into Petri-dishes filled with 0.2-µm filtered fresh seawater (FSW) prior to plating for spatial metabolomics. The tuft-shaped morphotype was dominated by *T. erythraeum* and the two puff-shaped morphotypes by *T. thiebautii* (17). The cultured *T. erythraeum* strain IMS101, originally isolated from the coastal waters of North Carolina in 1992 and obtained from the National Center for Marine Algae, was grown at 25°C, with a 10:14-hour light-dark cycle at ~80 µE m^{-2} s^{-1} in a modified YBC-II medium that contained 20 µM EDTA. Growth was monitored by measuring *in vivo* fluorescence. Culture aliquots containing free trichomes were harvested at mid-exponential growth. Cultured colonies formed at the end of the late stationary growth phase.

MALDI mass spectrometry imaging

Natural colony and cultured morphotype replicates were plated together on an indium tin oxide (ITO)-coated glass slide for matrix-assisted laser desorption/ionization mass

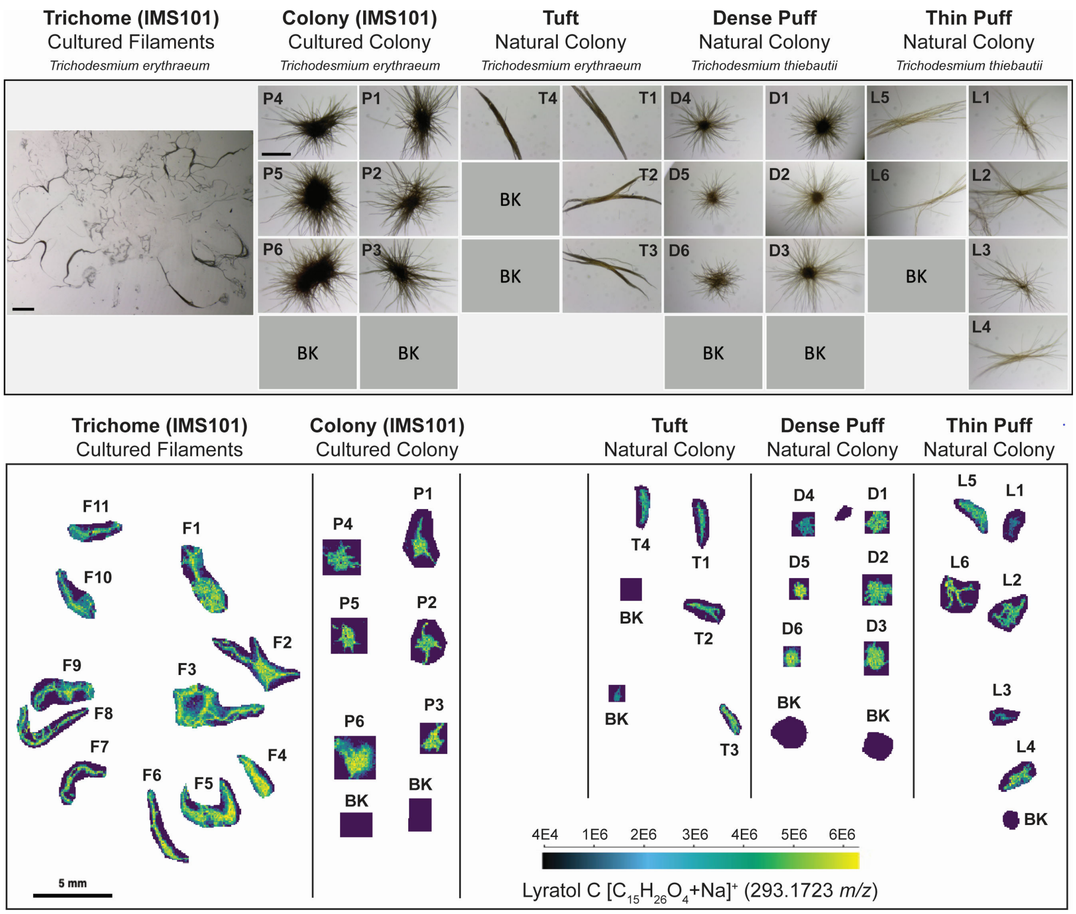

FIG 1 *Trichodesmium* morphotype replicate placement on an indium tin oxide-coated glass plate for MALDI-mass spectrometry imaging analysis showing images of cultured and natural colonies (top) and an example of the MALDI ion image for a detected feature (bottom). Morphotypes include cultured trichomes (F) and colonies (P) derived from the cultivable *T. erythraeum* strain IMS101. Natural colony morphotypes consist of *T. erythraeum* tuft-shaped colonies (T), and *T. thiebautii* dense puff (D) and thin puff (L) colonies collected from the Red Sea. Blank controls (BK) contain culture medium or 0.22-µm filtered fresh seawater from the point of colony collection. Scale bars in cultured trichome and colony images are 1 and 500 µm, respectively (top). Full-plate MALDI-MS ion intensity image (bottom) shows each morphotype replicate and absolute pseudo color scale for the detected sesquiterpenoid feature lyratol C $[C_{15}H_{26}O_4 + Na]^+$ (*m/z* 293.1723; 5% false discovery rate; Table 3).

spectrometry imaging (Fig. S1). All colony morphotype replicates were washed twice in FSW to reduce the salinity from 41 to 36 ppt. Each replicate was then placed on the slide, and residual seawater was wicked away with a lint-free wipe to minimize salt crusts that can form when the samples dry, which can interfere with instrument sensitivity. Individual colonies were photographed before and after placing on slides (Fig. 1). Once all colony and cultured morphotype replicates were placed on the ITO-coated glass slide, the slide was dried at 40°C overnight and stored at −20°C pending analysis. MALDI-MSI followed previously described methods (24). Briefly, MALDI matrix (2,5-dihydroxybenzoic acid (DHB): 40 mg/mL in 70% MeOH) was applied to the ITO-coated glass slide using an HTX TM-Sprayer (HTX Technologies) with the following spraying conditions: 12 passes with track spacing 3 mm, flow rate 50 µL/min, spray velocity 1,200 mm/min, spray pressure of 10 psi (N_2), and a 40-mm sprayer nozzle distance from the sample. Imaging was performed on a 15-tesla (T) MALDI-Fourier transform ion cyclotron resonance-mass spectrometer (SolariX, Bruker Daltonics) equipped with SmartBeam II laser source (355 nm, 2 kHz) in positive mode, using 200 shots at 2 kHz and a 200-µm step size. Each sample was analyzed by MALDI-FT-ICR using two settings: optimal for collection of low mass-to-charge (*m/z*) ions (92–500) and optimal for collection of high *m/z* ions (500–2,000). In low *m/z* mode, the instrument operated with 209 ms transient, achieving a mass resolution of ~130,000 at *m/z* 400. In high *m/z* mode, the instrument operated with 569 ms transient, achieving a mass resolution ~270,000 at *m/z* 400. As MALDI-MS is a surface-sensitive technique, the ion intensity values represent average intensities rather than the total signal across the colony surface area, effectively normalizing the data to the biomass surface area of each colony. MS imaging data were acquired using FlexImaging (v4.1, Bruker Daltonics), with image processing and visualization performed via SCiLS Lab (v2022a, Bruker Daltonics).

LESA tandem mass spectrometry

Additional colony and cultured morphotype replicates were plated together on a separate ITO-coated glass slide for liquid extraction surface analysis tandem mass spectrometry (Fig. S1). Seawater was wicked away from the slide surface with a lint-free wipe, and the plate was dried at 40°C overnight and stored at −20°C pending analysis. LESA-MS^2 was performed using a Triversa Nanomate (Advion) coupled to a Q-Exactive-Plus mass spectrometer (Thermo Scientific) operated in positive ion mode as previously described (24). Briefly, LESA sampling conditions were as follows: 8.0 µL of 70% MeOH was aspirated in the pipette tip, and then 0.3 µL of this volume was dispensed at a height of 0.2 mm above the sample surface. After a 1-second post-dispense delay, the volume was re-aspirated into the pipette tip and infused into the MS via nano-ESI. LESA sampling occurred serially with a 3-mm step size between probing areas. Each sample extraction location was sprayed into the MS for 4 min for iterative MS, and the top six ions were isolated for tandem MS^2 fragmentation analyses with a high-energy collisional dissociation energy of 30. LESA-MS^2 fragmentation data were analyzed via MetFrag to determine putative structures based on *in silico* scores (28).

Statistical approach

Shared features (i.e., metabolites) derived from MALDI-MSI were evaluated in METASPACE, which uses a false discovery rate (FDR) framework to calculate a metabolite-signal match (MSM) score and corresponding FDR estimate for each putative metabolite annotation by combining spectral and spatial measurements (29). The MSM score quantifies the likelihood of the presence of a known metabolite with a given sum formula in the group, where an MSM score of 1 indicates the maximal likelihood of the signal corresponding to a known metabolite in the database. Putative metabolite annotations were derived from the following METASPACE databases: the Chemical Entities of Biological Interest Database v2018-01 [ChEBI; (30)], the Human Metabolome Database v4 [HMDB; (31)], the Kyoto Encyclopedia of Genes and Genomes v1 [KEGG; (32)], and the Natural Products Atlas v2019-08 [NPA; (33)]. Shared features at the 5%, 10%, and 20% FDR thresholds were retained for downstream analysis. Differences in shared feature abundance were visualized using principal components analysis (PCA) ordination based on scaled intensity values (blank corrected) derived from each *Trichodesmium* morphotype replicate in R [v4.2.1; (34)]. Spatial discrimination analysis was applied to the MALDI-MSI data set to detect discriminant features between natural colony and cultured morphotypes. Specifically, an analysis of the receiver operating characteristics [ROC; (35)] was implemented as a univariate statistical approach using SciLS Lab (v2022a, Bruker Daltonics) to assess the discrimination quality of mass-to-charge values between any two groups. Here, all replicates of one natural colony or IMS101 culture morphotype were selected as one group and compared with all replicates of a second group. The area under the ROC curve (AUC) measures the discrimination quality in the interval between 0.0 and 1.0, where a perfect discrimination would yield an AUC equal to 0 or 1. The closer the AUC value is to 0.5, the less useful the feature, while the closer it is to 0.0 or 1.0, the more suitable the feature is to be used as a univariate criterion. The AUC threshold was set between 0.4 and 0.6 such that an AUC value exceeding 0.6 indicates substantially greater metabolite abundance in group 1 compared to group 2, while an AUC value below 0.4 indicates substantially lower metabolite abundance in group 1 compared to group 2. All AUC values between 0.4 and 0.6 were considered non-discriminant features and excluded from additional analysis. All remaining features were considered discriminant between *Trichodesmium* morphotypes in the spatial metabolomics analysis.

MetFrag, an *in silico* fragmenter workflow (28), was used to predict putative metabolite identification from the LESA-MS^2 fragmentation data for discriminant features derived from the MALDI-MSI analysis. The MetFrag workflow retrieves putative structures from compound databases, including ChEBI [v2018-01; (30)], HMDB [v4; (31)], KEGG [v1; (32)], and NPA [v2019-08; (33)]. These putative structures are then fragmented using a bond dissociation approach, and the fragments are compared with the product ions from the measured mass spectrum of the LESA-MS^2 data set to determine which structure best explains the measured data. The resulting structure scoring is a function of the *m/z* intensity and bond dissociation energy of the matched peaks, and a limited number of neutral loss rules that account for rearrangements (36). The putative structure with the best *in silico* statistical score was chosen to represent the predicted metabolite for all downstream annotation purposes.

RESULTS AND DISCUSSION

Here, we implement non-targeted metabolomics using ion image analysis following MALDI-MSI to detect 80 unique features (i.e., metabolites) across five *Trichodesmium* morphologies (Table S1). These include features at the 5%, 10%, and 20% false discovery rate thresholds with a mass-to-charge ratio accurate to within 0.6 ppm (24). This is the first untargeted analysis of small metabolites associated with morphologically distinct *Trichodesmium* colonies and could be expanded by an additional 1,686 features detected at the 50% FDR threshold following extensive visual verification to eliminate false-positive identification in METASPACE. When coupled with LESA-MS^2 fragmentation spectra, we not only contribute to the list of known metabolites associated with *Trichodesmium* but also corroborate the predicted molecular formula and putative molecule of each metabolite discovered to aid in future targeted metabolomics studies in bloom-forming *Trichodesmium* and ecosystems beyond.

Comparison of metabolites across morphotypes

Broad differences in the abundance of features between morphotypes were visualized using PCA ordination based on scaled ion intensity values derived from each *Trichodesmium* morphotype replicate (Fig. 2). Mean ion intensity values (blank corrected) for each feature by morphotype are provided in the supplemental materials (N = 80 features; Table S1). Differences in metabolite abundance between *Trichodesmium* morphotypes account for 43.6% of the variation (x-axis), while differences between replicates within each morphotype account for an additional 17.9% of the variation (y-axis; Fig. 2). There were three notable trends from the PCA ordination. First, natural colonies had similar metabolite profiles, resulting in an overlapping ordination between natural colony morphotypes (Fig. 2). Second, the metabolite profile of the cultured trichome morphotype differed from the cultured colony morphotype, with non-overlapping ordination between cultured morphotypes (Fig. 2). Third, the metabolite profile of the cultured colony morphotype exhibited a closer resemblance in feature abundance to the natural colony morphotypes compared to the cultured trichome morphotype, with non-overlapping ordination but a shift toward natural colony morphotypes (Fig. 2). This suggests that the transition from individual trichomes to the colony morphotype resulted in a production and abundance of features more similar to those found in natural colony morphotypes (Fig. 2). Moreover, it implies that the cultured IMS101 trichome morphotype is less representative of the metabolite composition and abundance observed in natural colony morphotypes.

To better understand which metabolites were driving this observed variation in the abundance of shared features between *Trichodesmium* morphotypes (Fig. 2), we performed a discrimination analysis on the 80 metabolites retained and verified for this study (29). Of these features, we detected 57 features that differed in MS ion intensity between natural and cultured *Trichodesmium* morphotypes (Table 1). The largest number

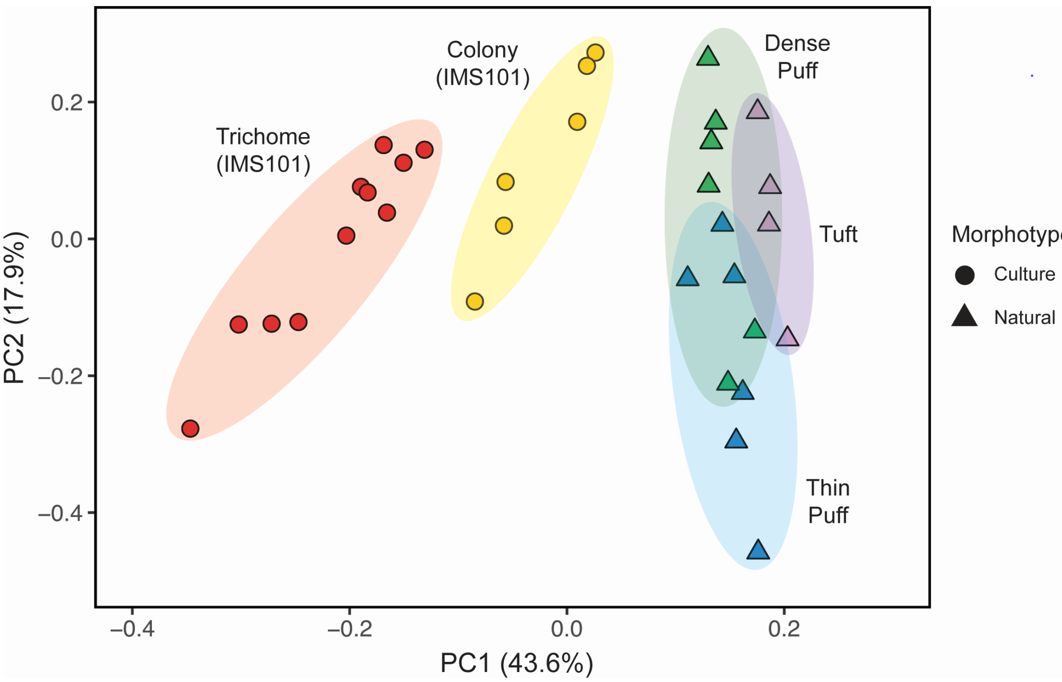

FIG 2 Principal components analysis ordination by morphotype based on scaled intensity values (blank corrected) derived from non-redundant shared features at the 5%, 10%, and 20% false discovery rate threshold in MALDI-MSI (N = 80 features). Distinct morphotypes are identified as follows: cultured trichome morphotype (red circles), cultured colony morphotype (yellow circles), natural dense puff colony morphotype (green triangles), natural thin puff colony morphotype (blue triangles), and natural tuft colony morphotype (purple triangles).

of discriminant features were observed between the cultured vs natural colonies as expected from our PCA ordination (Fig. 2). The cultured trichome morphotype had 29 features with greater ion intensity compared to all other morphotypes (Table 1). These features had the highest discriminant values (AUC) for most features when comparing their intensity with the natural colony morphotypes relative to the cultured colony morphotype (Table S2). In contrast, the tuft-shaped and dense puff natural colonies each had 23 features with greater ion intensity compared to either of the cultured IMS101 morphotypes, while the thin puff natural colony only had 14 features with greater ion intensity compared to either of the cultured IMS101 morphotypes (Table 1). In all three cases, the cultured trichome morphotype exhibits the lowest ion intensity for most of these features (Tables S3 and S4). This reflects the greater similarity of metabolites shared between natural colonies, regardless of morphotype, relative to the cultured colonies

TABLE 1 Summary of MALDI-MSI discriminant features between *Trichodesmium* morphologies[a]

Trichodesmium morphology	Discriminant features	5% FDR features	10% FDR features	20% FDR features
Cultured IMS101				
Cultured trichome	29	6	8	15
Cultured colony	2	0	0	2
Natural colonies				
Tuft-shaped colony	23	3	4	16
Dense puff colony	23	2	4	17
Thin puff colony	14	3	2	9
Total discriminant features	91	14	18	59
Non-redundant features	57	9	12	36

[a]The AUC threshold was set between 0.4 and 0.6 such that AUC values greater than 0.6 or less than 0.4 were considered discriminant features. Discriminant features are summarized based on putative metabolite annotations at the 5%, 10%, and 20% false discovery rate threshold.

as observed in our PCA ordination (Fig. 2) and highlights the extent of dissimilarity in shared metabolite abundance between cultured morphotypes and the natural colonies they are meant to represent.

Among the natural colony morphotypes, the dense puff and tuft-shaped morphotypes showed greater similarity in metabolite abundance compared to the thin puff morphotype (Fig. 2), where only eight features exhibited significant differences between the natural dense puff and tuft-shaped morphotypes (Table S3). In contrast, these two morphotypes shared 21 features with significantly greater abundance compared to the natural thin puff morphotype (Tables S3 and S4). This was surprising given that both puff-shaped morphotypes are dominated by *T. thiebautii*, while the tuft-shaped morphotype is dominated by *T. erythraeum* (17). This suggests that major differences between morphotype metabolism may be influenced by gene expression rather than variations in taxonomy.

Characterization of discriminant metabolites

The single-colony MALDI-MSI analysis conducted in this study enabled a comprehensive comparison of the abundance of annotated metabolites across distinct *Trichodesmium* morphotypes, highlighting the differences between cultured and natural colonies. Considering only features with the most confident molecular formula assignments (FDR ≤20%), our study identified 57 discriminant metabolites (Table 1) that differentiate distinct *Trichodesmium* morphotypes, prioritizing these metabolites for further characterization to determine how these molecules contribute to metabolic differences between *Trichodesmium* colonies.

Among the nine non-redundant discriminate features at the 5% FDR threshold (Table 1), six features had greater abundance in the cultured trichome morphotype compared to the cultured colony morphotype and all three natural colony morphotypes (Table 2; Fig. 3). Two of these features, including the putative sesquiterpenoid $C_{15}H_{28}O_4$ (M + Na$^+$; *m/z* 295.1879) and the putative monocarboxylic acid $C_{16}H_{28}O_6$ (M + Na$^+$; *m/z* 339.1778) (Table 3), were exclusively detected in the IMS101 trichome morphotype (Fig. 3). Four additional features were detected across all morphotypes but had greater abundance in the cultured trichome morphotype compared to the cultured colony morphotype and all three natural colony morphotypes (Table 2; Fig. 3). Two of these features were the putative dipeptide $C_{10}H_{16}N_2O_5$ (M + H$^+$; *m/z* 245.1132) and the nitrogen-rich purine like $C_{14}H_{20}N_6O_4$ (M + K$^+$; *m/z* 375.1177) (Table 3). The remaining two features, a putative sesquiterpenoid $C_{15}H_{26}O_4$ (M + Na$^+$; *m/z* 293.1723) and amino acid ester $C_{17}H_{24}N_2O_7$ (M + H$^+$; *m/z* 357.1656) also had the highest abundances in the IMS101 trichome morphotypes (Table 2), as illustrated by the pseudo color scale in the MALDI-MSI ion images (Fig. 3). Full-plate ion images showing each morphotype replicate and absolute logarithmic pseudo color scale for each feature (*m/z*) at the 5% FDR threshold are provided in the supplemental materials (Fig. S3 to S5).

There were an additional three non-redundant discriminant features at the 5% FDR threshold whose abundance was greater in the natural colony morphotypes compared to the cultured IMS101 morphotypes (Table 2; Fig. 4). The putative dipeptide $C_{14}H_{26}N_2O_4$ (M + Na$^+$; *m/z* 309.1784) was detected only in the natural thin puff and tuft morphotypes, while the remaining two metabolites, $C_{11}H_{20}N_2O_4$ (M + H$^+$; *m/z* 245.1495) and $C_{16}H_{27}N_2O_4$ (M + Na$^+$; *m/z* 320.1832) (Table 3), were detected in all three natural colony morphotypes (Fig. 4). However, these two metabolites were less abundant in the thin puff colonies than the dense puff or tuft morphotypes (Table 2; Fig. 4). The metabolite $C_{16}H_{27}N_2O_4$ (M + Na$^+$; *m/z* 320.1832) was putatively annotated as N-(3-oxododecanoyl)-homoserine lactone (3-oxo-C12-HSL) based on formula match in METASPACE (Table 3). 3-Oxo-C12-HSL is a specific type of acylated homoserine lactone (AHL) molecule involved in bacterial quorum sensing, playing a role in controlling motility, adhesion, and biofilm formation (37, 38).

At the 20% FDR threshold, an additional putative AHL molecule, N-hexanoyl-homoserine lactone (3-oxo-C6-HSL; $C_{10}H_{17}NO^3$ + H$^+$; *m/z* 200.1281), was found in all

TABLE 2 MALDI-MSI discriminant features at the 5% false discovery rate threshold[a]

Trichodesmium morphotype	Measured *m/z*	Predicted formula	Ion adduct	Area under the curve				
				vs Trichome (IMS101)	vs Colony (IMS101)	vs Tuft (natural)	vs Dense puff (natural)	vs Thin puff (natural)
Trichome (IMS101)	245.1132	$C_{10}H_{16}N_2O_5$	M + H	–[b]	**0.73**	**0.90**	**0.84**	**0.91**
	293.1723	$C_{15}H_{26}O_4$	M + Na	–	**0.68**	**0.68**	0.59	**0.68**
	295.1879	$C_{15}H_{28}O_4$	M + Na	–	**0.70**	**0.75**	**0.68**	**0.72**
	339.1778	$C_{16}H_{28}O_6$	M + Na	–	**0.77**	**0.80**	**0.78**	**0.79**
	357.1656	$C_{16}H_{24}N_2O_7$	M + H	–	**0.65**	0.56	0.53	**0.62**
	375.1177	$C_{14}H_{20}N_6O_4$	M + K	–	**0.62**	**0.69**	**0.63**	**0.71**
Tuft (natural)	245.1495	$C_{11}H_{20}N_2O_4$	M + H	**0.94**	**0.91**	–	0.54	**0.66**
	309.1784	$C_{14}H_{26}N_2O_4$	M + Na	**0.86**	**0.86**	–	**0.76**	**0.69**
	320.1832	$C_{16}H_{27}NO_4$	M + Na	**0.74**	**0.80**	–	0.46	0.56
Dense puff (natural)	245.1495	$C_{11}H_{20}N_2O_4$	M + H	**0.91**	**0.87**	0.46	–	**0.61**
	320.1832	$C_{16}H_{27}NO_4$	M + Na	**0.75**	**0.81**	0.54	–	**0.60**
Thin puff (natural)	245.1495	$C_{11}H_{20}N_2O_4$	M + H	**0.86**	**0.81**	**0.34**	**0.39**	–
	309.1784	$C_{14}H_{26}N_2O_4$	M + Na	**0.72**	**0.72**	**0.31**	**0.61**	–
	320.1832	$C_{16}H_{27}NO_4$	M + Na	**0.68**	**0.75**	0.44	**0.40**	–

[a]The AUC metric indicates discrimination quality in the interval between 0 and 1, where a perfect discrimination would yield an AUC equal to 0 or 1. The AUC threshold was set between 0.4 and 0.6 such that AUC values greater than 0.6 or less than 0.4 were considered discriminant features (bold). Putative classifications were derived from the corresponding databases available within METASPACE.
[b]The dash represents no comparison possible.

morphotypes (Table S1) and previously shown to promote biofilm and colony formation in cyanobacteria (39, 40). The osmolyte, homoserine betaine, $C_7H_{15}NO_3$ (M + H^+; *m/z* 162.1125), was more abundant in the IMS101 trichomes than the IMS101 colony or natural colony morphotypes (Table S2; Fig. S2) and previously characterized in the cultured IMS101 strain (41). Finally, an unidentified *Trichodesmium* iron chelator, $C_{15}H_{23}N_7O_5$ (M + H^+; *m/z* 382.1833), that was previously detected from *Trichodesmium* colonies in the Red Sea (42) was also detected in the natural *Trichodesmium* colonies from this study, predominantly the thin puff (Table S3) and tuft (Table S4) morphotypes but not from the cultivated IMS101 strain (Fig. S2).

Although there has been speculation that biopolymers, such as polysaccharides and glycans, contribute to adhesion and formation of *Trichodesmium* colonies, repeated saccharide units were not clearly detected by MALDI-MSI in this study. However, another biopolymer, the arginine-aspartate polymer cyanophycin, was detected as a series of ions differing by $C_{10}H_{17}N_5O_4$ (*m/z* 271.1230) exclusively in natural colonies as $C_{20}H_{36}N_{10}O_9$ (*m/z* 561.2722) and $C_{30}H_{53}N_{15}O_{13}$ (*m/z* 832.3952) (Fig. S2), differing by $C_{10}H_{17}N_5O_4$ (*m/z* 271.1230; Asp-Arg) as a series of ions (Fig. S6). Cyanophycin is commonly used as a nitrogen storage molecule in cyanobacteria, and putative cyanophycin granules have been previously observed in *Trichodesmium* IMS101 cultures (43). The results of our study indicated comparatively greater cyanophycin content in naturally occurring *Trichodesmium* colony morphotypes.

Structural predictions of metabolites

While MALDI-FT-ICR MS analyses identify specific metabolites at the molecular formula level that differentiate *Trichodesmium* morphotypes, it cannot discern between structural isomers of these molecules. To address this limitation, we utilized the complementary LESA-MS^2 approach to obtain fragmentation spectra for a subset of metabolites that provide a diagnostic fingerprint of specific molecular structures. In this study, we acquired fragmentation spectra for four discriminant features at the 5% FDR threshold, which were subsequently scored against isomers within the CheBI, HMDB, KEGG, and NPA databases using MetFrag (Fig. 5). Although fragmentation spectra were only obtainable for abundant features that ionized well by LESA, it provided putative structural annotations for these metabolites (24, 44).

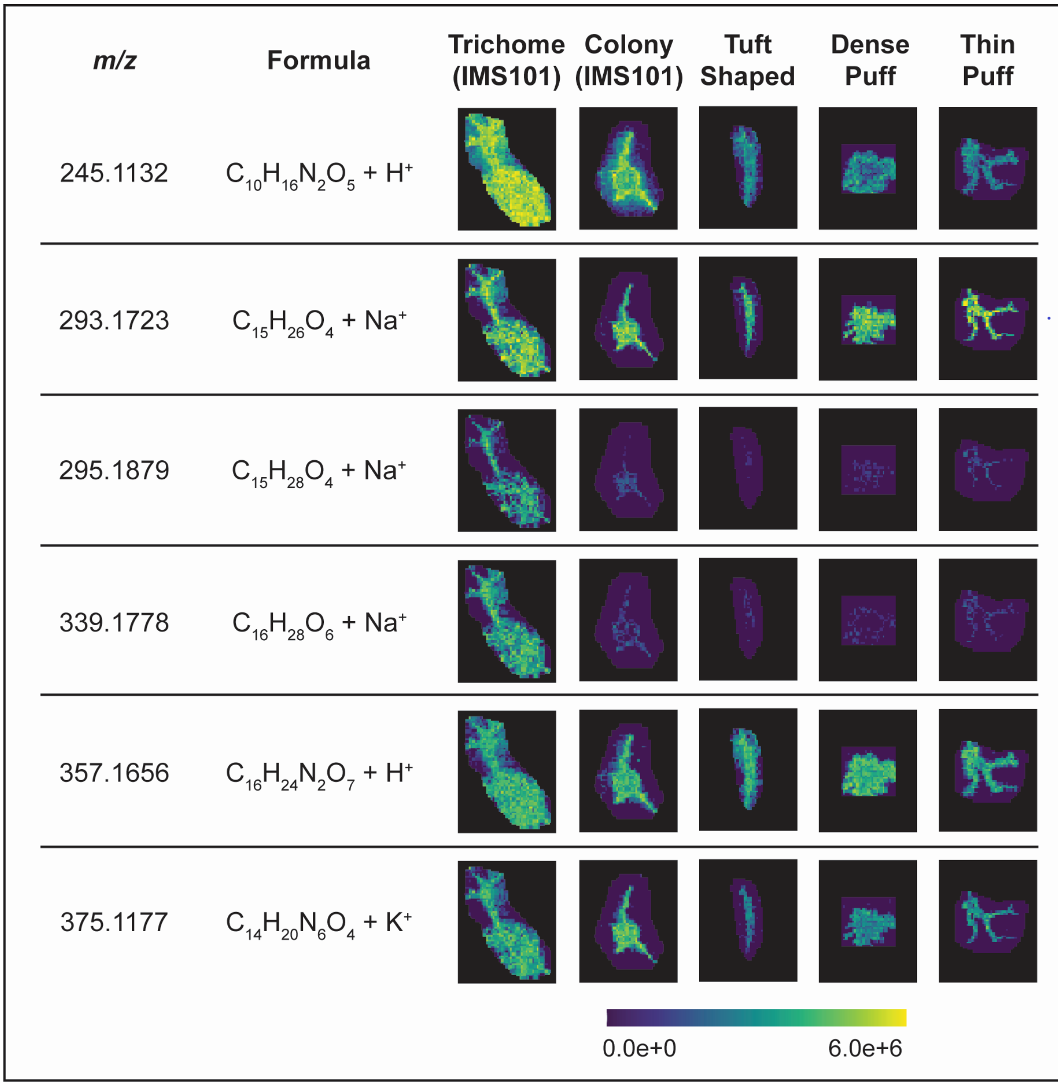

FIG 3 Ion images reconstructed from MALDI-MSI data illustrate the greater spatial abundance of discriminant features in the cultured trichome (IMS101) morphotype compared to all other morphotypes at the 5% false discovery rate threshold, as indicated in Table 2. An individual replicate for each *Trichodesmium* morphotype was consistently selected to represent the ion image for each discriminant feature, with each image visualized using an absolute logarithmic pseudo color scale of ion intensity. Full-plate ion images, depicting each morphotype replicate and absolute logarithmic pseudo color ion intensity values for each feature (*m/z*), can be found in Fig. S4 to S6 of the supplemental materials.

Specifically, LESA-MS^2 fragmentation spectra were obtained for the putative dipeptides $C_{11}H_{20}N_2O_4$ (*m/z* 245.1495; Fig. 5A) and $C_{14}H_{26}N_2O_4$ (*m/z* 309.1784, Fig. 5C), as well as for the putative sesquiterpenoid $C_{15}H_{26}O_4$ (*m/z* 293.1723; Fig. 5B) and the amino acid ester $C_{16}H_{24}N_2O_7$ (*m/z* 357.1656; Fig. 5D). Of three possible isomers and one isobar within the databases that matched the putative dipeptide $C_{11}H_{20}N_2O_4 + H^+$ (*m/z* 245.1495), LESA-MS^2 analysis supported hydroxyprolyl-isolucine as the most probable structure with the highest MetFrag *in silico* score of 71. The putative dipeptide $C_{14}H_{26}N_2O_4 + Na^+$ (*m/z* 309.1784) uniquely matched N-acetyl-leucyl-leucine in the databases. However, the low MetFrag score of 4 reflects the presence of additional fragments in the spectrum, suggesting potential structural discrepancies. Of two possible isomers for the putative sesquiterpenoid $C_{15}H_{26}O_4 + Na^+$ (*m/z* 293.1723), lyratol C exhibited the highest MetFrag *in silico* score of 109, making it the most probable molecular structure. The putative amino acid ester $C_{16}H_{24}N_2O_7 + H^+$ (*m/z* 357.1656) exclusively matched to pyriferine A in the database. This structural annotation was supported by a high MetFrag score of 167 (Fig. 5D).

TABLE 3 Putative annotations for MALDI-MSI discriminant features at the 5% false discovery rate threshold derived from the corresponding databases in METASPACE[a]

Measured m/z	Formula	Adduct	MSM	FDR	Database	MetFrag score	Putative classification	Putative annotation
Trichome								
245.1132	$C_{10}H_{16}N_2O_5$	M + H	0.92	5%	ChEBI	–[b]	Dipeptide	Glutamylproline
293.1723	$\mathbf{C_{15}H_{26}O_4}$	**M + Na**	**0.91**	**5%**	**ChEBI**	**109**	**Sesquiterpenoid**	**Lyratol C**
295.1879	$C_{15}H_{28}O_4$	M + Na	0.94	5%	ChEBI	–	Sesquiterpenoid	Alismorientol A
339.1778	$C_{16}H_{28}O_6$	M + Na	0.91	5%	ChEBI	–	Carboxylic acid	2,3,4,5-Tetranor-thromboxane B1
357.1656	$\mathbf{C_{16}H_{24}N_2O_7}$	**M + H**	**0.95**	**5%**	**NPA**	**167**	**Amino acid ester**	**Pyriferine A**
375.1177	$C_{14}H_{20}N_6O_4$	M + K	0.89	5%	ChEBI	–	Carboxylic acid	Adenosine-5′-(N-butyl) carboxamide
Natural colonies								
245.1495	$\mathbf{C_{11}H_{20}N_2O_4}$	**M + H**	**0.94**	**5%**	**HMDB**	**71**	**Dipeptide**	**Hydroxyprolyl-isoleucine**
309.1784	$\mathbf{C_{14}H_{26}N_2O_4}$	**M + Na**	**0.91**	**5%**	**KEGG**	**4**	**Dipeptide**	**N-acetyl-leucyl-leucine**
320.1832	$C_{16}H_{27}NO_4$	M + Na	0.93	5%	ChEBI	–	Carboxylic acid	N-(3-oxododecanoyl) homoserine lactone

[a]Putative annotations in **bold** were confirmed through LESA-MS^2 analysis based on MetFrag scores, with fragmentation spectra shown in Fig. 5.
[b]The dash indicates that no MetFrag score was available for that particular measured m/z feature.

Potential drivers of metabolite differences between morphotypes

Several factors may explain the metabolite differences between cultured morphotypes and natural colony morphotypes. Some metabolites likely reflect differences in the metabolic state of *Trichodesmium* related to colony formation. *Trichodesmium* are known to modify their metabolism in response to light, temperature, CO_2, metals, and nutrient concentrations, which differed between the lab and field (45, 46). The discriminant metabolite differences observed in this study between the IMS101 trichomes and their cultured colony morphology reflect metabolic changes as the cyanobacteria transition

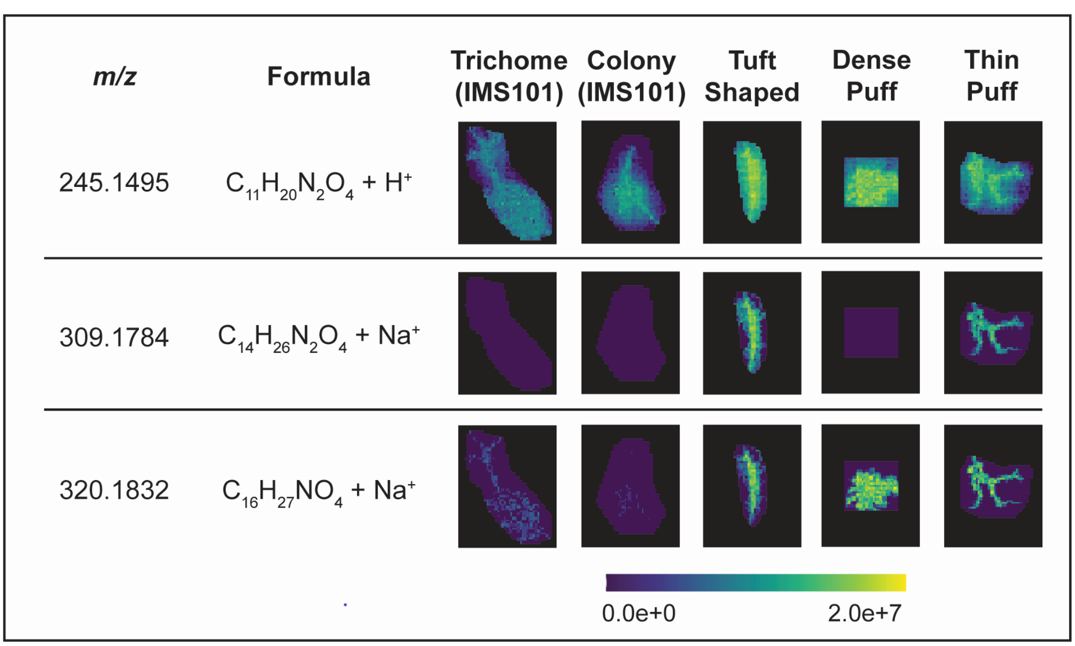

FIG 4 Ion images reconstructed from MALDI-MSI data illustrate the greater spatial abundance of discriminant features in the natural colony morphotypes compared to the cultured (IMS101) morphotypes at the 5% false discovery rate threshold as shown in Table 2. An individual replicate for each *Trichodesmium* morphotype was consistently selected to represent the ion image for each discriminant feature, with each image visualized using an absolute logarithmic pseudo color scale of ion intensity. Full-plate ion images showing each morphotype replicate and absolute logarithmic pseudo color ion intensity values for each feature (*m/z*) are shown in Fig. S4 and S5 of the supplemental materials.

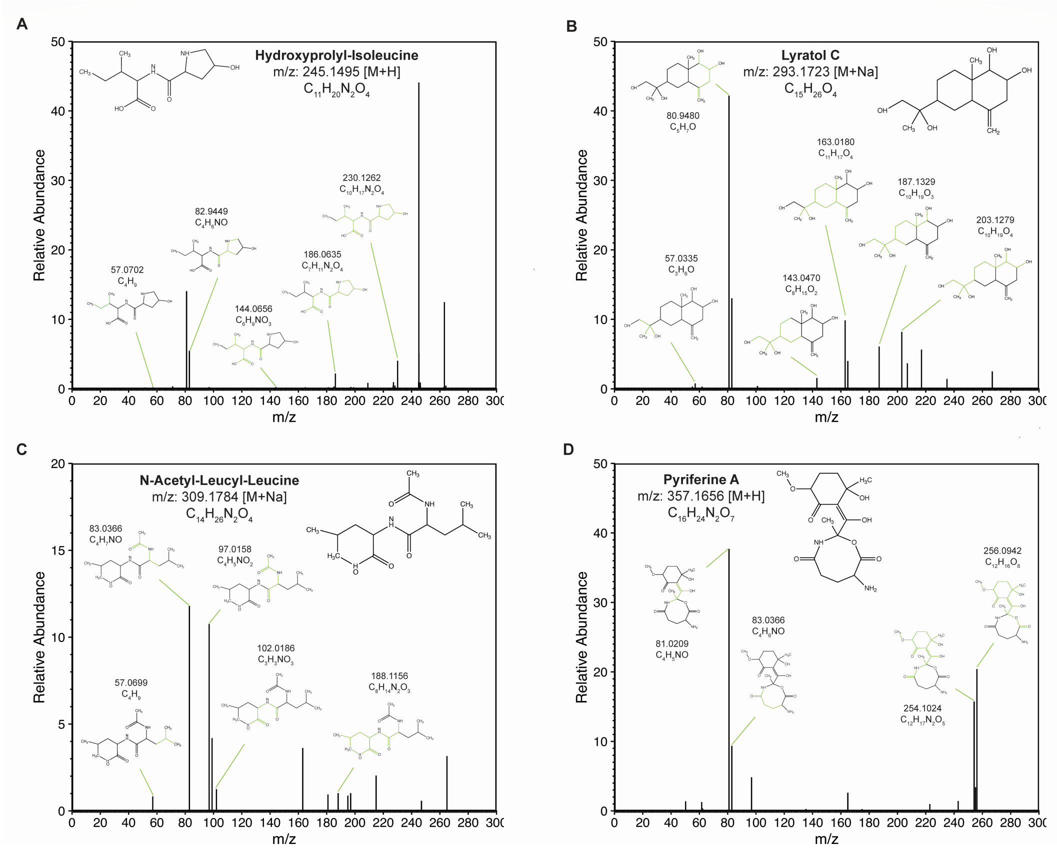

FIG 5 LESA-MS[2] fragmentation spectra corresponding to four MALDI-MSI discriminant features at the 5% false discovery rate threshold, including (A) hydroxyprolyl-isoleucine (*m/z* 245.1495), (B) lyratol C (*m/z* 293.1723), (C) N-acetyl-leucyl-leucine (*m/z* 309.1784), and (D) pyriferine A (*m/z* 357.1656).

from exponential growth to stationary phase. Differences between the laboratory and natural colonies likely also reflect similar physiological differences. For instance, the nitrogen storage peptide cyanophycin was exclusively observed in the natural colonies, although IMS101 is also capable of producing it (47). This suggests greater nitrogen storage by the natural colonies compared to the laboratory-grown colonies.

Another important difference between natural *Trichodesmium* colonies and cultured IMS101 trichomes involves the utilization of airborne dust as a source of iron, an important micronutrient in large parts of the ocean (7, 48, 49). Single IMS101 trichomes do not form stable associations with dust (15), while natural colonies from the Red Sea, Sargasso Sea, and the Atlantic Ocean were repeatedly observed to capture, translocate, and pack dust particles in their cores and utilize them to amend their high iron demands for photosynthesis and N_2-fixation (7, 50, 51). In IMS101 cultures, the shift between individual trichomes and colony lifestyle was also found to result in strong interactions with dust (15). Both the aggregation into a stable colony structure and the tendency to adhere to dust should involve the production of surface metabolites and as such likely reveal a distinct chemical fingerprint for dust utilization following the formation of certain colony morphotypes. Further characterization of discriminant metabolites shared between the cultured IMS101 colony morphotype and natural colony morphotypes may reveal which surface metabolites are involved in dust utilization.

Some differences between the dense and thin puff natural colonies are also likely related to metabolic state. Recent genetic analysis of natural colony morphotypes collected from the Red Sea has shown that puff-shaped morphotypes are predominantly associated with the same species of *T. thiebautii*, suggesting that morphotype differences are related to gene regulation rather than distinct physiological capabilities (17).

For example, the two dipeptides, putatively annotated as hydroxyprolyl-isoleucine (*m/z* 245.1495) and N-acetyl-leucyl-leucine (*m/z* 309.1784), that were less abundant in the thin puff colonies (Table 2; Fig. 4) may reflect such differences. Recent research comparing natural *Trichodesmium* morphotypes from the Red Sea further revealed that the thin puff morphotype exhibits a significantly higher activity in capturing, translocating, and packaging dust particles in its core compared to the dense puff morphotype (19). This activity likely allows thin puff *Trichodesmium* morphotypes to extract essential nutrients, such as iron and phosphorus, from dust particles deposited on ocean surface waters, leaving dense puff morphotypes metabolically vulnerable to the high demands of these micronutrients for photosynthesis and N_2-fixation (7, 50, 51). Consequently, the 21 features showing discriminately greater abundance in the dense puff morphotype relative to the thin puff morphotype (Table S3) could serve as promising candidates for targeted metabolomics studies aimed at elucidating their role in dust centering activity in response to nutrient stress.

Alternatively, some metabolite differences may reflect the distinct genetic capabilities of different colony morphotypes, attributed either to the *Trichodesmium* species or their co-existing epibionts. Puff-shaped morphotypes in the Red Sea are predominantly associated with *T. thiebautii*, whereas recent genetic analysis has shown that tuft-shaped morphotypes are dominated by *T. erythraeum* (17). Pangenomic analyses of *Trichodesmium* clades have revealed significant differences in genetic capabilities, with only about one-quarter of genes shared among all species (17, 52). Previous research has also demonstrated that natural *Trichodesmium* colony morphotypes in the Red Sea, including puffs and tufts, exhibit a comparable composition of marine epibionts, regardless of variations in *Trichodesmium* species composition and morphologies (22). These epibionts are likely distinct from those associated with cultivatable IMS101 morphotypes (53–55). For example, differences in epibiont activity are likely related to the higher production of the putative quorum-sensing AHL, 3-oxo-C12-HSL, in the natural colonies compared to the cultured colonies (56). AHLs have been reported to be produced by epibiotic bacteria associated with natural *Trichodesmium* colonies for use in quorum sensing to regulate the activity of alkaline phosphatases (APases) used to acquire phosphate from dissolved organic phosphorus molecules (19, 57). Another field study testing transcriptional changes of natural *Trichodesmium* microbiomes to AHL addition revealed differential expression of genes related to energy metabolism, chemotaxis, motility and attachment, and nitrogen and amino acid metabolism functional groups (58). It is likely that AHLs found in this study contribute to colony formation and communication among members of the natural *Trichodesmium* colonies, but more research is needed to elucidate the role of these specific compound targets.

Conclusions and future perspectives

MALDI-MSI at single-colony resolution allowed us to confidently detect and localize a greater diversity of small metabolites (80 confirmed + >1,600 potential metabolites) produced within and between natural and cultured *Trichodesmium* morphotypes than has been previously achieved. The combination of MALDI-MSI with LESA-MS^2 fragmentation analysis further provided greater confidence that putative classifications and annotations for MALDI features represented the most likely molecular formula and structure. By investigating the spatial distribution of discriminant features across natural and cultured *Trichodesmium* morphotypes, we identified specific distinctions between the metabolite profile of the cultivatable *T. erythraeum* strain IMS101 and natural colony morphotypes collected from the Red Sea. The formation of culture colonies led to a shift in their metabolite profile toward the metabolite profile shared between the natural colony morphotypes. These results suggest that the cultured colony morphotype could be a better cultivatable proxy for natural *Trichodesmium* colonies in laboratory-based incubation experiments compared to trichomes. In addition, we found key metabolites that differed between distinct colony morphotypes from the Red Sea.

Overall, the metabolite profiles of natural and cultured *Trichodesmium* colonies remain understudied in comparison to what is known about their ecological role as dominant marine diazotrophs that form extensive surface blooms in oligotrophic ocean regions. Knowing how morphological differences between *Trichodesmium* colonies may contribute to measured differences in nutrient uptake, resilience, adaptability, flexibility, and the production and release of organic molecules through metabolite production remain an important component for modeling ocean biogeochemical cycles. The 57 discriminant features shared among *Trichodesmium* morphotypes identified in this study represent an initial step in associating specific molecular masses, formulae, and putative structures with distinct colony morphotypes. Beyond the metabolites annotated in METASPACE, there were many unannotated metabolite *m/z* values detected by MALDI-MSI that were in some cases strongly discriminant between natural morphotypes. These findings offer promising candidates for future targeted metabolomic investigations that provide mechanistic insights into the functional differences between *Trichodesmium* colony morphotypes.

ACKNOWLEDGMENTS

The authors wish to thank Dr. Coco Koedooder, Dr. Subhajit Basu, Murielle Dray, and Emanuel Sestieri for technical support. This research was performed under the Facilities Integrating Collaborations for User Science (FICUS) program (10.46936/fics.proj.2018.50403/60000053) and used resources at the Environmental Molecular Sciences Laboratory, a DOE Office of Science User Facility sponsored by the Biological and Environmental Research program and operated under contract nos. DE-AC02-05CH11231 (JGI) and DE-AC05-76RL01830 (EMSL). This research was supported by grant no. 2020041 awarded to Y.S. and R.M.B. from the United States-Israel Binational Science Foundation (BSF), and grant no. 621513 awarded to R.M.B. from the Simons Foundation. F.Z. acknowledges the PBC postdoctoral fellowship for Chinese researchers from Israel (2020–22).

F.Z., R.M.B., and Y.S. conceived the study. F.Z. and S.W. collected natural *Trichodesmium* colonies from the Red Sea. F.Z. and S.W. cultured IMS101 and formed its colonies in the laboratory. F.Z. prepared MALDI-MSI and LESA-MS^2 slides and photographed colonies. D.V. and R.K.C. processed the MALDI-MSI and LESA-MS^2 plates and provided the spatial metabolomics data sets. Under the guidance of R.M.B. and D.V., K.J.R. analyzed the spatial metabolomics data set. The manuscript was written by K.J.R., with contributions and feedback from F.Z., S.W., D.V., R.K.C., Y.S., and R.M.B. All authors contributed to the article and approved the submitted version.

AUTHOR AFFILIATIONS

[1]College of Earth, Ocean, and Atmospheric Sciences, Oregon State University, Corvallis, Oregon, USA
[2]Fredy and Nadine Hermann Institute of Earth Sciences, Hebrew University, Jerusalem, Israel
[3]The Interuniversity Institute for Marine Sciences, Eilat, Israel
[4]Environmental Molecular Sciences Laboratory, Pacific Northwest National Laboratory, Richland, Washington, USA
[5]Department of Chemistry, University of Minnesota, Minneapolis, Minnesota, USA

AUTHOR ORCIDs

Karl J. Romanowicz http://orcid.org/0000-0001-8732-3272
Dušan Veličković http://orcid.org/0000-0001-7945-9620
Rene M. Boiteau http://orcid.org/0000-0002-4127-4417

FUNDING

Funder	Grant(s)	Author(s)
U.S. Department of Energy (DOE)	DE-AC02-05CH11231	Dušan Veličković Rosalie K. Chu Yeala Shaked Rene M. Boiteau
U.S. Department of Energy (DOE)	DE-AC05-76RL01830	Dušan Veličković Rosalie K. Chu Yeala Shaked Rene M. Boiteau
United States-Israel Binational Science Foundation (BSF)	2020041	Yeala Shaked Rene M. Boiteau
Simons Foundation (SF)	621513	Rene M. Boiteau

AUTHOR CONTRIBUTIONS

Karl J. Romanowicz, Data curation, Formal analysis, Investigation, Writing – original draft, Writing – review and editing | Futing Zhang, Conceptualization, Data curation, Investigation, Methodology, Writing – review and editing | Siyuan Wang, Conceptualization, Data curation, Investigation, Writing – review and editing | Dušan Veličković, Data curation, Formal analysis, Methodology, Resources, Validation, Writing – review and editing | Rosalie K. Chu, Data curation, Formal analysis, Methodology, Resources, Validation, Writing – review and editing | Yeala Shaked, Conceptualization, Data curation, Funding acquisition, Investigation, Methodology, Project administration, Resources, Supervision, Writing – review and editing | Rene M. Boiteau, Conceptualization, Data curation, Formal analysis, Funding acquisition, Investigation, Methodology, Project administration, Resources, Software, Supervision, Validation, Visualization, Writing – original draft, Writing – review and editing

DATA AVAILABILITY

Metabolites derived from MALDI-MSI are publicly available for viewing and downloading from METASPACE: https://metaspace2020.eu/project/Romanowicz2024. Data associated with LESA-tandem MS^2 fragmentation analysis are available in the MassIVE repository: https://massive.ucsd.edu/ProteoSAFe/dataset.jsp?accession=MSV000093569.

ADDITIONAL FILES

The following material is available online.

Supplemental Material

Supplemental Material (mSystems01152-24-s0001.pdf). Tables S1 to S4 and Figures S1 to S6.

Open Peer Review

PEER REVIEW HISTORY (review-history.pdf). An accounting of the reviewer comments and feedback.

REFERENCES

1. Capone DG, Burns JA, Montoya JP, Subramaniam A, Mahaffey C, Gunderson T, Michaels AF, Carpenter EJ. 2005. Nitrogen fixation by *Trichodesmium* spp.: an important source of new nitrogen to the tropical and subtropical north Atlantic Ocean. Glob Biogeochem Cycles 19. https://doi.org/10.1029/2004GB002331
2. Gruber N, Sarmiento JL. 1997. Global patterns of marine nitrogen fixation and denitrification. Global Biogeochem Cycles 11:235–266. https://doi.org/10.1029/97GB00077

3. Mahaffey C, Michaels AF, Capone DG. 2005. The conundrum of marine N2 fixation. Am J Sci 305:546–595. https://doi.org/10.2475/ajs.305.6-8.546
4. Capone DG, Zehr JP, Paerl HW, Bergman B, Carpenter EJ. 1997. *Trichodesmium*, a globally significant marine cyanobacterium. Science 276:1221–1229. https://doi.org/10.1126/science.276.5316.1221
5. Sohm JA, Mahaffey C, Capone DG. 2008. Assessment of relative phosphorus limitation of *Trichodesmium* spp. in the north Pacific, north Atlantic, and the north coast of Australia. Limnol Oceanogr 53:2495–2502. https://doi.org/10.4319/lo.2008.53.6.2495
6. Eichner M, Inomura K, Pierella Karlusich JJ, Shaked Y. 2023. Better together? Lessons on sociality from *Trichodesmium*. Trends Microbiol 31:1072–1084. https://doi.org/10.1016/j.tim.2023.05.001
7. Rubin M, Berman-Frank I, Shaked Y. 2011. Dust- and mineral-iron utilization by the marine dinitrogen-fixer *Trichodesmium*. Nature Geosci 4:529–534. https://doi.org/10.1038/ngeo1181
8. Tzubari Y, Magnezi L, Be'er A, Berman-Frank I. 2018. Iron and phosphorus deprivation induce sociality in the marine bloom-forming cyanobacterium *Trichodesmium*. ISME J 12:1682–1693. https://doi.org/10.1038/s41396-018-0073-5
9. Mulholland MR, Capone DG. 1999. Nitrogen fixation, uptake and metabolism in natural and cultured populations of *Trichodesmium* spp. Mar Ecol Prog Ser 188:33–49. https://doi.org/10.3354/meps188033
10. Klawonn I, Eichner MJ, Wilson ST, Moradi N, Thamdrup B, Kümmel S, Gehre M, Khalili A, Grossart HP, Karl DM, Ploug H. 2020. Distinct nitrogen cycling and steep chemical gradients in *Trichodesmium* colonies. ISME J 14:399–412. https://doi.org/10.1038/s41396-019-0514-9
11. Hewson I, Poretsky RS, Dyhrman ST, Zielinski B, White AE, Tripp HJ, Montoya JP, Zehr JP. 2009. Microbial community gene expression within colonies of the diazotroph, *Trichodesmium*, from the southwest Pacific Ocean. ISME J 3:1286–1300. https://doi.org/10.1038/ismej.2009.75
12. Berman-Frank I, Bidle KD, Haramaty L, Falkowski PG. 2004. The demise of the marine cyanobacterium, *Trichodesmium* spp., via an autocatalyzed cell death pathway. Limnol Oceanogr 49:997–1005. https://doi.org/10.4319/lo.2004.49.4.0997
13. Bell PRF, Uwins PJR, Elmetri I, Phillips JA, Fu F-X, Yago AJE. 2005. Laboratory culture studies of *Trichodesmium* isolated from the great barrier reef Lagoon, Australia. Hydrobiologia 532:9–21. https://doi.org/10.1007/s10750-004-8768-1
14. Hynes AM, Webb EA, Doney SC, Waterbury JB. 2012. Comparison of cultured *Trichodesmium* (Cyanophyceae) with species characterized from the field. J Phycol 48:196–210. https://doi.org/10.1111/j.1529-8817.2011.01096.x
15. Kessler N, Armoza-Zvuloni R, Wang S, Basu S, Weber PK, Stuart RK, Shaked Y. 2020. Selective collection of iron-rich dust particles by natural *Trichodesmium* colonies. ISME J 14:91–103. https://doi.org/10.1038/s41396-019-0505-x
16. Eichner MJ, Klawonn I, Wilson ST, Littmann S, Whitehouse MJ, Church MJ, Kuypers MM, Karl DM, Ploug H. 2017. Chemical microenvironments and single-cell carbon and nitrogen uptake in field-collected colonies of *Trichodesmium* under different pCO_2 ISME J 11:1305–1317. https://doi.org/10.1038/ismej.2017.15
17. Koedooder C, Landou E, Zhang F, Wang S, Basu S, Berman-Frank I, Shaked Y, Rubin-Blum M. 2022. Metagenomes of red sea subpopulations challenge the use of marker genes and morphology to assess *Trichodesmium* diversity. Front Microbiol 13:879970. https://doi.org/10.3389/fmicb.2022.879970
18. Eichner M, Kranz SA, Rost B. 2014. Combined effects of different CO2 levels and N sources on the diazotrophic cyanobacterium *Trichodesmium*. Physiol Plant 152:316–330. https://doi.org/10.1111/ppl.12172
19. Wang S, Koedooder C, Zhang F, Kessler N, Eichner M, Shi D, Shaked Y. 2022. Colonies of the marine cyanobacterium *Trichodesmium* optimize dust utilization by selective collection and retention of nutrient-rich particles. i Sci 25:103587. https://doi.org/10.1016/j.isci.2021.103587
20. Sheridan CC, Steinberg DK, Kling GW. 2002. The microbial and metazoan community associated with colonies of *Trichodesmium* spp.: a quantitative survey. J Plankton Res 24:913–922. https://doi.org/10.1093/plankt/24.9.913
21. Rouco M, Haley ST, Dyhrman ST. 2016. Microbial diversity within the *Trichodesmium* holobiont. Environ Microbiol 18:5151–5160. https://doi.org/10.1111/1462-2920.13513
22. Koedooder C, Zhang F, Wang S, Basu S, Haley ST, Tolic N, Nicora CD, Glavina Del Rio T, Dyhrman ST, Gledhill M, Boiteau RM, Rubin-Blum M, Shaked Y. 2023. Taxonomic distribution of metabolic functions in bacteria associated with *Trichodesmium* consortia. mSystems 8:e0074223. https://doi.org/10.1128/msystems.00742-23
23. Dilillo M, Ait-Belkacem R, Esteve C, Pellegrini D, Nicolardi S, Costa M, Vannini E, Graaf EL de, Caleo M, McDonnell LA. 2017. Ultra-high mass resolution MALDI imaging mass spectrometry of proteins and metabolites in a mouse model of glioblastoma. Sci Rep 7:603. https://doi.org/10.1038/s41598-017-00703-w
24. Veličković D, Chu RK, Carrell AA, Thomas M, Paša-Tolić L, Weston DJ, Anderton CR. 2018. Multimodal MSI in conjunction with broad coverage spatially resolved MS^2 increases confidence in both molecular identification and localization. Anal Chem 90:702–707. https://doi.org/10.1021/acs.analchem.7b04319
25. Boya P. CA, Fernández-Marín H, Mejía LC, Spadafora C, Dorrestein PC, Gutiérrez M. 2017. Imaging mass spectrometry and MS/MS molecular networking reveals chemical interactions among cuticular bacteria and pathogenic fungi associated with fungus-growing ants. Sci Rep 7:1–13. https://doi.org/10.1038/s41598-017-05515-6
26. Khalil SM, Pretzel J, Becker K, Spengler B. 2017. High-resolution AP-SMALDI mass spectrometry imaging of drosophila melanogaster. Int J Mass Spectrom 416:1–19. https://doi.org/10.1016/j.ijms.2017.04.001
27. Eikel D, Vavrek M, Smith S, Bason C, Yeh S, Korfmacher WA, Henion JD. 2011. Liquid extraction surface analysis mass spectrometry (LESA-MS) as a novel profiling tool for drug distribution and metabolism analysis: the terfenadine example. Rapid Commun Mass Spectrom 25:3587–3596. https://doi.org/10.1002/rcm.5274
28. Wolf S, Schmidt S, Müller-Hannemann M, Neumann S. 2010. In silico fragmentation for computer assisted identification of metabolite mass spectra. BMC Bioinformatics 11:1–12. https://doi.org/10.1186/1471-2105-11-148
29. Palmer A, Phapale P, Chernyavsky I, Lavigne R, Fay D, Tarasov A, Kovalev V, Fuchser J, Nikolenko S, Pineau C, Becker M, Alexandrov T. 2017. FDR-controlled metabolite annotation for high-resolution imaging mass spectrometry. Nat Methods 14:57–60. https://doi.org/10.1038/nmeth.4072
30. Hastings J, Owen G, Dekker A, Ennis M, Kale N, Muthukrishnan V, Turner S, Swainston N, Mendes P, Steinbeck C. 2016. ChEBI in 2016: improved services and an expanding collection of metabolites. Nucleic Acids Res 44:D1214–9. https://doi.org/10.1093/nar/gkv1031
31. Wishart DS, Feunang YD, Marcu A, Guo AC, Liang K, Vázquez-Fresno R, Sajed T, Johnson D, Li C, Karu N, et al. 2018. HMDB 4.0: the human metabolome database for 2018. Nucleic Acids Res 46:D608–D617. https://doi.org/10.1093/nar/gkx1089
32. Kanehisa M, Furumichi M, Tanabe M, Sato Y, Morishima K. 2017. KEGG: new perspectives on genomes, pathways, diseases and drugs. Nucleic Acids Res 45:D353–D361. https://doi.org/10.1093/nar/gkw1092
33. van Santen JA, Jacob G, Singh AL, Aniebok V, Balunas MJ, Bunsko D, Neto FC, Castaño-Espriu L, Chang C, Clark TN, et al. 2019. The natural products atlas: an open access knowledge base for microbial natural products discovery. ACS Cent Sci 5:1824–1833. https://doi.org/10.1021/acscentsci.9b00806
34. R Core Team. 2013. R: a language and environment for statistical computing
35. Pepe MS. 2000. Receiver operating characteristic methodology. J Am Stat Assoc 95:308–311. https://doi.org/10.1080/01621459.2000.10473930
36. Ruttkies C, Schymanski EL, Wolf S, Hollender J, Neumann S. 2016. MetFrag relaunched: incorporating strategies beyond *in silico* fragmentation. J Cheminform 8:3. https://doi.org/10.1186/s13321-016-0115-9
37. Mireille Ayé A, Bonnin-Jusserand M, Brian-Jaisson F, Ortalo-Magné A, Culioli G, Koffi Nevry R, Rabah N, Blache Y, Molmeret M. 2015. Modulation of violacein production and phenotypes associated with biofilm by exogenous quorum sensing N-acylhomoserine lactones in the marine bacterium *Pseudoalteromonas ulvae* TC14. Microbiology (Reading) 161:2039–2051. https://doi.org/10.1099/mic.0.000147
38. Liu J, Fu K, Wang Y, Wu C, Li F, Shi L, Ge Y, Zhou L. 2017. Detection of diverse N-acyl-homoserine lactones in *Vibrio alginolyticus* and regulation

of biofilm formation by N-(3-Oxodecanoyl) homoserine lactone *in vitro*. Front Microbiol 8:250966. https://doi.org/10.3389/fmicb.2017.01097
39. Sharif DI, Gallon J, Smith CJ, Dudley ED. 2008. Quorum sensing in cyanobacteria: N-octanoyl-homoserine lactone release and response, by the epilithic colonial cyanobacterium gloeothece PCC6909. ISME J 2:1171–1182. https://doi.org/10.1038/ismej.2008.68
40. Herrera N, Echeverri F. 2021. Evidence of quorum sensing in cyanobacteria by homoserine lactones: the origin of blooms. Water (Basel) 13:1831. https://doi.org/10.3390/w13131831
41. Pade N, Michalik D, Ruth W, Belkin N, Hess WR, Berman-Frank I, Hagemann M. 2016. Trimethylated homoserine functions as the major compatible solute in the globally significant oceanic cyanobacterium *Trichodesmium*. Proc Natl Acad Sci U S A 113:13191–13196. https://doi.org/10.1073/pnas.1611666113
42. Gledhill M, Basu S, Shaked Y. 2019. Metallophores associated with *Trichodesmium erythraeum* colonies from the Gulf of Aqaba. Metallomics 11:1547–1557. https://doi.org/10.1039/c9mt00121b
43. Finzi-Hart JA, Pett-Ridge J, Weber PK, Popa R, Fallon SJ, Gunderson T, Hutcheon ID, Nealson KH, Capone DG. 2009. Fixation and fate of C and N in the cyanobacterium *Trichodesmium* using nanometer-scale secondary ion mass spectrometry. Proc Natl Acad Sci U S A 106:6345–6350. https://doi.org/10.1073/pnas.0810547106
44. Nagy G, Veličković D, Chu RK, Carrell AA, Weston DJ, Ibrahim YM, Anderton CR, Smith RD. 2019. Towards resolving the spatial metabolome with unambiguous molecular annotations in complex biological systems by coupling mass spectrometry imaging with structures for lossless ion manipulations. Chem Commun (Camb) 55:306–309. https://doi.org/10.1039/c8cc07482h
45. Shi T, Sun Y, Falkowski PG. 2007. Effects of iron limitation on the expression of metabolic genes in the marine cyanobacterium *Trichodesmium erythraeum* IMS101. Environ Microbiol 9:2945–2956. https://doi.org/10.1111/j.1462-2920.2007.01406.x
46. Levitan O, Brown CM, Sudhaus S, Campbell D, LaRoche J, Berman-Frank I. 2010. Regulation of nitrogen metabolism in the marine diazotroph *Trichodesmium* IMS101 under varying temperatures and atmospheric CO2 concentrations. Environ Microbiol 12:1899–1912. https://doi.org/10.1111/j.1462-2920.2010.02195.x
47. Miyakawa T, Yang J, Kawasaki M, Adachi N, Fujii A, Miyauchi Y, Muramatsu T, Moriya T, Senda T, Tanokura M. 2022. Structural bases for aspartate recognition and polymerization efficiency of cyanobacterial cyanophycin synthetase. Nat Commun 13:5097. https://doi.org/10.1038/s41467-022-32834-8
48. Basu S, Shaked Y. 2018. Mineral iron utilization by natural and cultured *Trichodesmium* and associated bacteria. Limnol Oceanogr 63:2307–2320. https://doi.org/10.1002/lno.10939
49. Basu Subhajit, Gledhill M, de Beer D, Prabhu Matondkar SG, Shaked Y. 2019. Colonies of marine cyanobacteria *Trichodesmium* interact with associated bacteria to acquire iron from dust. Commun Biol 2:284. https://doi.org/10.1038/s42003-019-0534-z
50. Rueter JG, Hutchins DA, Smith RW, Unsworth NL. 1992. Iron nutrient of *Trichodesmium,* p 289–306. In Marine pelagic cyanobacteria: *Trichodesmium* and other diazotrophs
51. Held NA, Sutherland KM, Webb EA, McIlvin MR, Cohen NR, Devaux AJ, Hutchins DA, Waterbury JB, Hansel CM, Saito MA. 2021. Mechanisms and heterogeneity of in situ mineral processing by the marine nitrogen fixer *Trichodesmium* revealed by single-colony metaproteomics. ISME Commun 1:35. https://doi.org/10.1038/s43705-021-00034-y
52. Webb EA, Held NA, Zhao Y, Graham ED, Conover AE, Semones J, Lee MD, Feng Y, Fu FX, Saito MA, Hutchins DA. 2023. Importance of mobile genetic element immunity in numerically abundant *Trichodesmium* clades. ISME Commun 3:15. https://doi.org/10.1038/s43705-023-00214-y
53. Lee M.D., Walworth NG, McParland EL, Fu FX, Mincer TJ, Levine NM, Hutchins DA, Webb EA. 2017. The *Trichodesmium consortium*: conserved heterotrophic co-occurrence and genomic signatures of potential interactions. ISME J 11:1813–1824. https://doi.org/10.1038/ismej.2017.49
54. Lee Michael D, Webb EA, Walworth NG, Fu F-X, Held NA, Saito MA, Hutchins DA. 2018. Transcriptional activities of the microbial consortium living with the marine nitrogen-fixing cyanobacterium *Trichodesmium* reveal potential roles in community-level nitrogen cycling. Appl Environ Microbiol 84:e02026-17. https://doi.org/10.1128/AEM.02026-17
55. Hou S, López-Pérez M, Pfreundt U, Belkin N, Stüber K, Huettel B, Reinhardt R, Berman-Frank I, Rodriguez-Valera F, Hess WR. 2018. Benefit from decline: the primary transcriptome of *Alteromonas macleodii* str. Te101 during *Trichodesmium* demise. ISME J 12:981–996. https://doi.org/10.1038/s41396-017-0034-4
56. Frischkorn Kyle R, Rouco M, Van Mooy BAS, Dyhrman ST. 2017. Epibionts dominate metabolic functional potential of *Trichodesmium* colonies from the oligotrophic ocean. ISME J 11:2090–2101. https://doi.org/10.1038/ismej.2017.74
57. Van Mooy BAS, Hmelo LR, Sofen LE, Campagna SR, May AL, Dyhrman ST, Heithoff A, Webb EA, Momper L, Mincer TJ. 2012. Quorum sensing control of phosphorus acquisition in *Trichodesmium consortia.* ISME J 6:422–429. https://doi.org/10.1038/ismej.2011.115
58. Frischkorn KR, Rouco M, Mooy BA, Dyhrman ST. 2018. The *Trichodesmium* microbiome can modulate host N2 fixation. Limnol Oceanogr Lett 3:401–408. https://doi.org/10.1002/lol2.10092